CRUSTAL DEFORMATION IN NW IRAN: INSIGHTS FROM DIFFERENT INVARIANT AND VARIANT COMPONENTS OF GEODETIC STRAIN RATE TENSORS

M. Rahmani[1*], V. Nafisi[1], J. Asgari[1], A. Nadimi[2]

[1] Dept. of Geomatics Engineering, Faculty of Civil Engineering and Transportation, University of Isfahan, Isfahan, Iran - (mi.rahmani, nafisi, asgari) @eng.ui.ac.ir
[2] Dept. of Geology, University of Isfahan, Isfahan, Iran - a.nadimi@sci.ui.ac.ir

Commission IV, WG IV/3

KEY WORDS: Arabia-Eurasia convergence, NW Iran, Shape deformation, GPS, Geodetic strain rate tensors, North Tabriz Fault (NTF).

ABSTRACT:

Northwest of Iran, as a tectonically active region, has experienced numerous devastating earthquakes. That is why it is so important to study the earth deformation in this area and to provide more precise insights. So far, most researchers have had the preference of using the invariant component of strain rate tensor for investigating the Earth's shape deformation in the region. However, to examine the efficiency of the variant components of the geodesic strain rate tensor in interpreting deformations of north-western Iran, we have in this article maps of variant components of the geodetic strain rate tensor (normal strain rate along north and eastbound). Using the velocity field gathered from a previous article, and also using a simple and straightforward method, the strain rate tensors were calculated. The obtained contraction along the north direction (from the normal strain along this axis) confirms the Eurasia-Arabia collision. Besides, the obtained extension along the east direction and the derived expansion of the dilatation, show the effect of Anatolian motion to the west and eastward movement of the central Iran plateau on the tectonic structure of the studied area. These two results showed that the variant component of strain rate tensor also provides us with useful information about a region shape deformation.

1. INTRODUCTION

The N-S collision between the Arabian and Eurasian plate has formed various complicated structural features in western Iran and eastern Turkey (Malekshahian, Naeeni, 2018). Hence, NW Iran and eastern Turkey are prominent places in the investigation of the influence of Arabian-Eurasia collision (Djamour et al., 2011). Besides, many earthquakes have taken place in NW Iran: Varzaghan-Ahar earthquakes in 2011 (6.5 M_w and 6.3 M_w) and Hashtrude earthquake in November 2019 (5.9 M_w), Figure 1; therefore, providing more accurate tectonic knowledge in NW Iran is extremely important to find points of high seismic potential.

Modern space geodetic techniques, including GPS, have been used for monitoring earth deformation. Following the 2003 Bam earthquake which struck the Kerman province in the southeast of Iran, the National Cartographic Center of Iran (NCC) settled a permanent network of GPS observation site throughout Iran to estimate the velocity field progressively (Vernant et al., 2004; Khorrami et al., 2019). It is interesting to notice that some parts of this network, in particular, NW Iran have a high density of stations (Masson et al., 2014; Malekshahian, Naeeni, 2018).

Several articles have been carried out using a GPS-deduced velocity field on crustal deformation on a large scale in Iran (e.g., Malekshahian, Naeeni, 2018; Khorrami et al., 2019). Though, in some articles, the authors investigated the local tectonic effect in NW Iran (Djamour et al., 2011). The integration of several types of data was applied in some other publications to compute crustal deformation in NW Iran: Su et al. (2016) utilized a combination of GPS and InSAR techniques data; Zarifi et al. (2014) applied the seismic and GPS data. It is evident that applying a variety of datasets together can increase our knowledge of shape deformations in a region.

So far, using the GPS network, several approaches have been taken to calculate strain rate tensor in NW Iran (Malekshahian, Naeeni, 2018; Khorrami et al., 2019). While in most previous publications the invariant components of strain rate tensors (principal strain rate, dilatation, and maximum shear strain rate) were calculated and employed to investigate this region shape deformation, this study aims to examine the feasibility of using variant components of geodetic strain rate tensor as a complement of invariant ones to developed understanding of crustal deformation in NW of Iran. To do achieve the goal, first, a different, fast and straightforward method in terms of computation, and GPS geodetic measurements are applied. Next, like most previous tectonic studies, invariant components of strain rate tensors are computed and interpreted; as well as the invariant components, variant elements of strain rate tensor (normal strain rate along east and north-axis) are derived and explained.

2. THE SEISMOTECTONIC FRAMEWORK OF NW IRAN

Our case study is located between the south of the Caucasus and the west of the Caspian Basin (Talesh Mountains). Jackson et al. (2002) (based on seismological data) and Masson et al. (2006) (using geodetic data), reported a N-S strike-slip motion in the western neighborhood of the Caspian Sea, and NNE-SSW extension within the Talesh plateau. The western border of the

* Corresponding author

case study corresponds to the westerly moving Anatolian plateau (Jackson 1992). As a result of the convergence between the Arabia and Eurasia plates, the Anatolian plateau was forced westward, and central Iran was ejected eastward (Su et al., 2017; Khorrami et al., 2019). The Anatolian motion to the west is known as a classic example of escape or extrusion (Gürbüz, Şaroğlu, 2018).

North Tabriz Fault (NTF) is a right-lateral strike-slip fault within NW Iran. Previous studies (e.g., Nilforoushan et al., 2003; Masson et al., 2006; Khorrami et al., 2019) proposed the right-lateral strike-slip motion along the Tabriz fault; this statement is shown in Figure 1(a), supported by the focal mechanism data[1]; furthermore, Figure 1(a) shows a reverse right-lateral oblique motion in the western part of this fault and the north of Lake Urmia (LU); this feature has been described in the previous publications (e.g. Su et al., 2017). In this figure the red and orange lines are active faults so that Astara-F and Talesh-F stand for Astara fault and Talesh fault, respectively. The earthquake mechanism solutions also indicate thrust motion along the Talesh plateau; this result was reported by Jackson et al. (2002). In summary, the deformation of NW Iran is controlled by the Eurasia-Arabia collision and several local tectonic motion resulting from this collision.

The results presented by Djamour et al. (2011) and Su et al. (2017) using geodetic data showed that NTF is seismically active. Numerous strong earthquakes have struck NW Iran, in particular, the region around NTF. After Varzaghan-Ahar earthquake sequences (6.5 M_w and 6.3 M_w) that occurred on August 11, 2012, no devastating seismic event was recorded in NW Iran for years; see Karimzadeh et al. (2013). But recently, a 5.9 M_w earthquake struck the area around Hashtrud (a city in East Azerbaijan Province), and two 5.7 M_w and 5.9 M_w earthquakes hit the region around Ghator (in West Azerbaijan Province and near the Iran-Turkey border) (Table 1).

Earthquake location	Magnitude (M_w)	Depth (km)	Date
Hashtrude	5.9	19	2019.11.07
Ghator	5.7	6	2020-02-23
Ghator	5.9	12	2020-02-23

Table 1[2] . The last largest earthquake in NW Iran.

Figure 1(b) shows the distribution of seismic events with $M_w \geq 4$ from 1980 to 2017; the different color shows the depth of seismic events, and the circle size is in proportion to earthquake magnitude. Yellow stars are representative of the Hashtrud earthquake and its aftershocks, while red stars depict Ghator seismic events. Black star represents Varzaghan-Ahar earthquake. It is apparently seen that a large percentage of earthquakes have always taken place along the Tabriz fault, especially in the western and northern part of this fault. It is worth noticing that the north part of this fault was considered to be a rigid block by Djamour et al. (2011); whereas, according to Masson et al. (2006) it was considered to be extending. Moreover, most of the earthquakes are shallow (usually less than 30 km deep) and have a magnitude of $4 \leq M_w < 5$.

The information presented in Table 1 clearly indicates that the Hashtrud and Ghator earthquakes are restricted to the depths less than 30 km, in agreement with the statements stated earlier. The focal mechanism of the 2019 November 7 Hashtrud earthquakes (the yellow color focal mechanism in Figure 1(a)) and the 2020 February 23 Ghator earthquakes (red focal mechanism in Figure 1(a)), depict a right-lateral strike-slip motion: similar to the majority of the previous earthquakes along NTF.
The historical background of NW Iran earthquakes (before the Hashtrud earthquakes) illustrates that two segments have had the potentiality of having devastating earthquakes: one segment was the region that the Hashtrud earthquake was taken place over, and the other was the rectangular area surrounded by the solid black line in Figure 1(b); hence, understanding the tectonic behavior of this region and NTF is highly important.

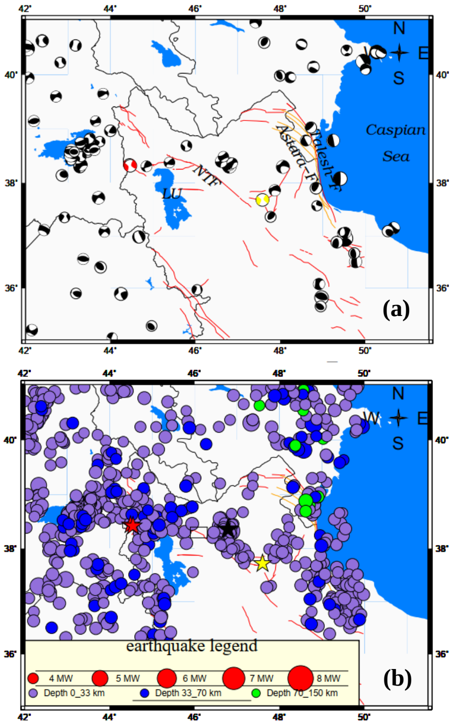

Figure 1. (a) Earthquake focal mechanism in the study area from 1980 to 2017 for $M_w \geq 4$. (b) Epicenter earthquake location in NW Iran from 1980 to 2017.

3. DATA AND METHOD OF CALCULATING STRAIN RATE

In this article, the GPS-derived velocity field of NW Iran has been gathered from a previous study, which was done by Zarifi et al. (2014). These velocity vectors are plotted in Figure 2; this figure reveals that the distribution of stations is homogeneous over the study area.

The main idea of the method used for calculating strain rates in NW Iran can be summarized as follows. (v_E^i, v_N^i) i =1: n, represents the horizontal velocity of the involving stations as observation sites. Here, to calculate strain rate tensors at each site, all stations within a distance less than 200 km are considered the observation sites. To access this threshold (200 km) first, the spherical distance between each couple of station was computed using the Eq.1, where r is the spherical radius of the earth, φ_i and φ_j represent latitude of the involved stations, and $\Delta\lambda_{ij}$ indicates

[1] http://www.globalcmt.org/CMTsearch.html
[2] https://www.emsc-csem.org/Earthquake/europe/M4/

the difference between the longitude of i and j (Goudarzi et al., 2015).

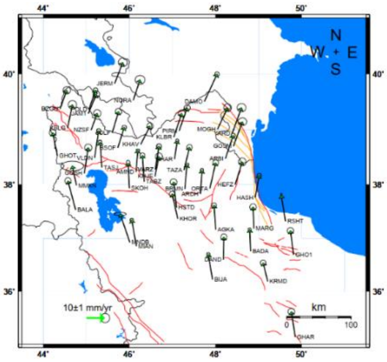

Figure 2. Map of the GPS velocity vectors (with respect to Eurasia-fixed frame (EURA_I08)) and their corresponding 95% confidence level ellipses.

The results represented that the mean value of the distances between these sites is approximately 167 km; although, in the computation of the strain rate tensor using the Eq.2, at least three observation sites are necessary; this required condition has been reached almost at all stations with considering 200 km as the threshold value.

$$R_{ij} = r\cos^{-1}(\sin\varphi_i \sin\varphi_j + \cos\varphi_i \cos\varphi_j \cos\Delta\lambda_{ij}) \quad (1)$$

Components of strain rate tensor ($\dot{\varepsilon}_{EE}$, $\dot{\varepsilon}_{EN}$, $\dot{\varepsilon}_{NN}$) at each site, with coordinates of E_m,N_m, are linked with the measured velocity (v_E^i, v_N^i) at the observation sites by the following relationships.

$$\begin{bmatrix} v_E^1 \\ v_N^1 \\ v_E^2 \\ v_N^2 \\ \vdots \\ v_E^n \\ v_N^n \end{bmatrix} = \begin{bmatrix} 1 & E_1 - E_m & N_1 - N_m & 0 & 0 & 0 \\ 0 & 0 & 0 & 1 & E_1 - E & N_1 - N_m \\ 1 & E_2 - E_m & N_2 - N_m & 0 & 0 & 0 \\ 0 & 0 & 0 & 1 & E_2 - E_m & N_2 - N_m \\ \vdots & \ddots & & & & \vdots \\ 1 & \cdots & N_n - N_m & 0 & 0 & 0 \\ 0 & 0 & 0 & 1 & E_n - E_m & N_n - N_m \end{bmatrix} \begin{bmatrix} a_0 \\ a_1 \\ a_2 \\ b_0 \\ b_1 \\ b_2 \end{bmatrix} \quad (2)$$

Eq. 2 is rewritten in the following form and unknown parameters can be determined:

$$y = Ax \rightarrow \hat{x} = \begin{bmatrix} \hat{a}_0 \\ \hat{a}_1 \\ \hat{a}_2 \\ \hat{b}_0 \\ \hat{b}_1 \\ \hat{b}_2 \end{bmatrix} = A^{-1}y \quad (3)$$

$$\dot{\varepsilon} = \begin{bmatrix} \dot{\varepsilon}_{EE} & \dot{\varepsilon}_{EN} \\ \dot{\varepsilon}_{NE} & \dot{\varepsilon}_{NN} \end{bmatrix} = \begin{bmatrix} \hat{a}_1 & \frac{1}{2}(\hat{a}_2 + \hat{b}_1) \\ \frac{1}{2}(\hat{a}_2 + \hat{b}_1) & \hat{b}_2 \end{bmatrix} \quad (4)$$

Here, a_0, a_1, a_2 are considered to explain velocity in east direction, while b_0, b_1, b_2 are used to defined velocity in north direction. a_0 and b_0 are translation unknown while others are unknown for velocity gradient.

It is evident that the strain rate tensor is symmetric. Eigenvalues of this two-dimensional tensor represent the minimum and maximum principal strain rates (Cai, Grafarend, 2007). These parameters are invariant of the strain rate tensor:

$$\boldsymbol{\lambda}_{1,2} = \frac{1}{2}\left(\dot{\varepsilon}_{EE} + \dot{\varepsilon}_{NN} \pm \sqrt{(\dot{\varepsilon}_{EE} - \dot{\varepsilon}_{NN})^2 + 4\dot{\varepsilon}_{EN}^2}\right), \quad \boldsymbol{\lambda} \in \mathbb{R} \quad (5)$$

The principal angle can be computed using Eq. 6; if we rotate the strain tensor to the degree of the principal angle, then the shear component would be set to zero (Cai, Grafarend, 2007).

$$\alpha = \frac{1}{2}\tan^{-1}\left(\frac{2\dot{\varepsilon}_{EN}}{\dot{\varepsilon}_{EE} - \dot{\varepsilon}_{NN}}\right) \quad -\boldsymbol{\pi/2} < \alpha \leq \boldsymbol{\pi/2} \quad (6)$$

The rotation is can be calculated using the next equation:

$$\text{Rotation} = \left(\frac{1}{2}(\hat{a}_2 - \hat{b}_1)\right) \quad (7)$$

In two dimensions, dilatation provides information about the relative variation of a surface area:

$$\dot{\varepsilon}_{\text{area}} = \dot{\varepsilon}_{EE} + \dot{\varepsilon}_{NN} = (\lambda_1 + \lambda_2) \quad (8)$$

The final parameter is known as the maximum shear strain rate:

$$\dot{\varepsilon}_{\text{max shear}} = (\lambda_1 - \lambda_2) \quad (9)$$

It is worth mentioning that both dilatation and maximum shear strain rate are invariant components of strain rate tensor, because these are the linear combination of eigenvalues.

4. RESULTS

In addition to invariant components of the strain rate tenor, variants were also examined in this article to explore the feasibility of using variant components as complements of invariants. The first part of this section focuses on the invariant components, while the second part focuses on variant components results.

4.1. Invariant Components of Strain Rate Tensors

In the following, first of all, the obtained principal strain rates and rotation are reported, and then dilatation and maximum-shear strain rate are discussed in detail.

4.1.1. Principal Strain Rate and Rotation Rate

The distribution of the geodetic principal strain rates in NW Iran is shown in Figure 3. In this figure the arrow outward demonstrates tensile, and the inward one indicates compressive. Red and orange lines denote the active faults in the studied area. As shown in the illustration, and as it was mentioned earlier in previous GPS researches (e.g., Zarifi et al., 2014; Malekshahian, Naeeni, 2018; Khorrami et al., 2019), the orientation of the obtained extension and compression rate axis is NE-SW and NW-SE, respectively. Considering the obtained motion and Figure 3(b), along the existed faults in this region (especially NTF) a right-lateral strike-slip motion might be concluded. The right-lateral slip rate of the Anatolian plateau could play a role in the right-lateral strike-slip motion in north-western Iran (Jackson, McKenzie, 1984).

In the northwest part of the study area, larger extension and compression strain rates, related to the southeast of the region are observed; furthermore, extension strain rates are larger than compression ones in the eastern part of the region, including east of Tabriz Fault. In contrast, in the western part of this region, especially the western part of NTF, both components are roughly equalled; this agrees with the results proposed by Masson et al. (2007) and Khorrami et al. (2019). The highest values of the compressive (~-26 ppb/yr) and extensive (~25 ppb/yr) strain rates have been derived at MMKN (longitude=44.7710˚E; latitude=37.9850˚N) and BALA stations, respectively; both sites belong to the western part of the network and near Iran-Turkey border.

As mentioned earlier, the mechanism of most earthquakes in this area is right-lateral strike-slip; it reports that there are NE-SW extensive and NW-SE compressive strain rates in this region; this result reveals a good agreement with the direction of geodetic and seismic principal strain rates.

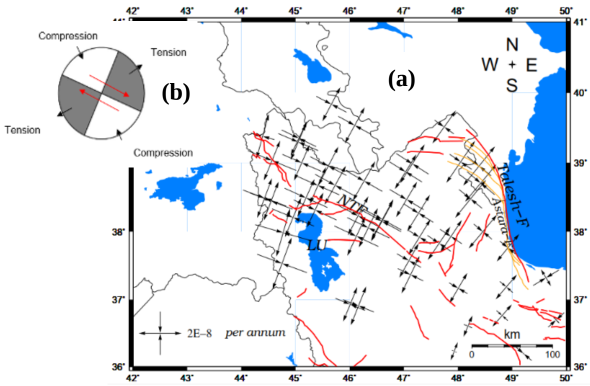

Figure 3. (a) The deduced direction of maximum principal axes of strain rates. (b) focal mechanism of a right-lateral strike-slip motion.

A glance at Figure 4 (with considering positive rotation equivalent to clock-wise rotation) reveals clock-wise rotation in this region. Maximum rotation (approximately 2.4904e-08 radian per annum) has been found in the west of LU (at the MMKN station); on the contrary, minimum rotation (~3.4802e-09 radian per annum) has been found at KRMD site (central part of Iran). That's to say, the rotation of the western part of this region is more prominent than other parts. The maximum rotation achieved near the Iran-Turkish border can be attributed to the west-moving Anatolian Plateau.

4.1.2. Dilatation Rate and Maximum Shear Strain Rate

In addition to the principal strain rate and rotation, dilatation rate and maximum-shear strain rate, have been computed and provided in Figure 5.

According to most of the previous geodynamic researches that have been conducted in large-scale Iran (Malekshahian, Naeeni, 2018), contraction is observed in a large percentage of Iran, particularly NW Iran. This contraction is mainly due to the Arabia-Eurasia collision and a small extension reported in NW Iran; see Masson et al. (2006).

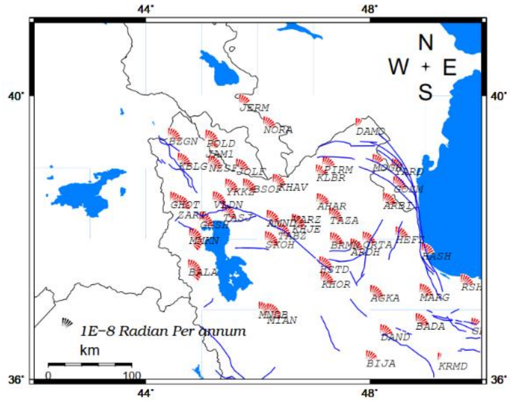

Figure 4. Map of the rotation rates in NW Iran.

Though, our results from the local NW network show expansion in most parts of this region and small shortening in the western part of the study area, Iran-Turkey border, and the south of Caspian Sea (Alborz Mountains), see Figure 5(a). As pointed out before, the focal mechanism data shows reverse motion in the western part of NTF; hence, using geodetic measurements, the obtained contraction in this area represents good consistency between geodetic and seismic results.

Despite the expansion in the east of the Tabriz fault, a small contraction is observed in the western part of this fault. However, the obtained expansion in the east of the case study is compatible with the geological structure of this region: the north-south shortening between the south of Caspian Sea and Central part of Iran, and the right-lateral strike-slip motion along a north-south fault bordering the western Caspian coast (Talesh plateau and Astara Fault) (Copley, Jackson, 2006; Masson et al., 2007; Zarifi et al., 2014). Also, the maximum expansion is equalled to 11.3783 ppb/yr and occurs at MOGH station (longitude = 48.0490˚E, latitude = 39.0130˚N). The Obtained shortening in the southern part of the Caspian Sea is consistent with the Caspian Basin and Arabia plate convergence; Jackson et al. (2002) and Walpersdorf et al. (2014) pointed out the shortening in Alborz.

Eventually, these results confirm that as well as the convergence between Arabia and Eurasia plate, NW Iran tectonic structure is controlled by the Caspian Sea, Kura basin (Rastbood, Voosoghi, 2011), NTF, and Talesh Fault (Malekshahian, Naeeni, 2018) as regional effects.

The maximum-shear strain rate of this region decreases from north and west to the other parts, refer to Figure 5(b); in agreement with Malekshahian, Naeeni (2018) and Khorami et al. (2019) consequences. It is evident from Figure 5(b) that shear strain in the western part of Tabriz Fault is more noticeably related to the eastern part of this fault. The maximum value of this parameter (~50 ppb/yr) arises in the western part of the Tabriz Fault and Iran-Turkey territory (at the longitude of MMKN and BALA). There is a good consistency between the obtained shear strain, geological, and tectonic structure of this area, particularly westerly moving of the Anatolian plateau due to the Arabia-Eurasia collision.

4.2. Variant Components of Strain Rate Tensors

In the following, a description of the variant component of strain rate tensor, including Normal strain rate along both east and north-axis is provided.

The normal strain rate map along the east-axis is illustrated in Figure 6(a). It depicts that major parts of the region extend along the east-axis, and this extension increases from east to west; so that the maximum value (~20 ppb/yr) is taken place near the Iran-Turkey border (BALA and MMKN sites). The obtained extension in the majority part of the study area is mainly due to the westerly escape of the Anatolian plateau and eastward ejection of central Iran.

However, in the south Caspian Basin, compression along the east-axis is found; the maximum of this compression (~-8 ppb/yr) has been recognized in RSHT (the nearest site to the south of the Caspian Basin). Also, the western border of the Caspian Basin (Talesh Mountain) shows a small extension. To summarize, normal strain along the east-axis reveals east-west extension in NW Iran.

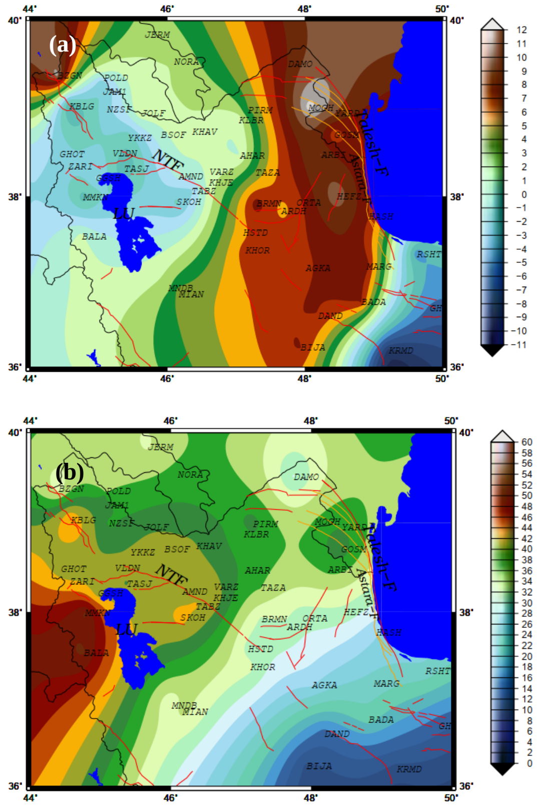

Figure 5. (a) surface dilatation rate. (b) Surface maximum-shear rates in the NW Iran (all values represented in part per billion per year).

The normal strain rate along the north-axis (Figure 6(b)) shows compression in most parts of this area, and similar to extension behaviour along the east-axis, the compression increases from east to west. This consequence is compatible with the Eurasia-Arabia convergence. Maximum compression along the north-axis (~-23 ppb/yr) occurs at MMKN station. However, in the western border Caspian Basin and south of it, a small extension is observed; the maximum extension (~3 ppb/yr) belongs to RSHT.

In conclusion, while a large percentage of NW Iran is extended along the east-axis and compressed along the north-axis, RSHT (north most station in the south of Caspian Basin) reveals compression (along the east-axis) and extension (along the north-axis).

5. DISCUSSION

The calculated dilatation rate (in section 4.1) reflects expansion and contraction which originated mostly stem from local tectonic motion, regardless of the direction of the change.

On the other hand, the variant components of strain rate tensors (normal strain rates along east and north direction) provide good results: (1) The obtained contraction along the north direction highlights the Eurasia-Arabia collision and (2) the observed extension along the east-axis in the majority part of the study area mainly reflects the westerly escape of the Anatolian plateau and eastward ejection of central Iran. These two movements are not shown in the estimated dilation rate. Therefore, it seems that the variant components can be considered a good addition to the dilation rate in NW Iran.

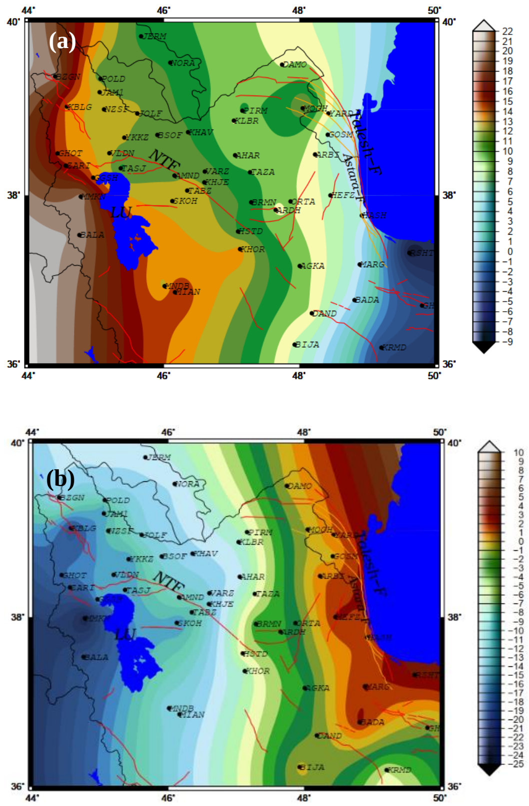

Figure 6. (a) Normal strain rate along the x-axis. (b) Normal strain rate along the y-axis. All values reported in part per billion per year (ppb/yr).

We recommend examining the efficiency of these variant components for monitoring earth deformation in NW Iran using InSAR observations. The next recommendation is to study the behaviour of these parameters on a larger scale, for example across Iran.

6. CONLUSIONS

In this study, using the determined velocity field by Zarifi et al. (2014), we presented the crustal deformation in NW Iran.

The behavior of the invariant parameters, in particular, dilatation and maximum-shear strain rate changes, clearly imply the role of local tectonic effect: (1) westerly moving of the Anatolian plateau might be the reason for the maximum value of rotation and maximum-shear strain rate in the western part of the network. (2) If it is assumed that this region is only controlled by Arabia-Eurasia collision, then NW Iran would be expected to be shortening; at the same time, our results show both contraction and expansion: significant expansion in the east of Tabriz fault, and the small contraction in the western part of this fault. The north-south shortening between the south part of the Caspian Sea and the Central part of Iran, and also the right-lateral strike-slip motion along a north-south fault bordering the western Caspian coast (Talesh plateau and Astara Fault), play an important role in the obtained expansion.

Besides, the invariant component of strain rate tensor, the variant components of strain rate tensor present useful knowledge of NW Iran tectonic: (1) the extension along the x-axis approves the westerly escape of the Anatolian plateau and eastward ejection of central Iran; (2) the obtained shortening along the y-axis confirms the N-W convergence of Arabia and Eurasia plateau. A comparison among our results, and the mechanism of the study area earthquakes clearly show a good agreement in terms of the extensional and compressional strain rates direction. Finally, our geodetic results and the focal mechanism of the earthquakes, approve the mentioned right-lateral strike-slip motion in the previous papers.

REFERENCES

Cai, J., Grafarend, E. W., 2007. Statistical analysis of geodetic deformation (strain rate) derived from the space geodetic measurements of BIFROST Project in Fennoscandia. *Journal of Geodynamics*, 43, 214-238.

Copley, A., Jackson, J., 2006. Active tectonics of the Turkish-Iranian plateau. *Tectonics*, 25.

Djamour, Y., Vernant, P., Nankali, H. R., Tavakoli, F., 2011. NW Iran-eastern Turkey present-day kinematics: results from the Iranian permanent GPS network. *Earth and Planetary Science Letters*, 307, 27-34.

Goudarzi, M. A., Cocard, M., Santerre, R., 2015. GeoStrain: An open source software for calculating crustal strain rates. *Computers & Geosciences, 82, 1-12.*

Gürbüz, A., Şaroğlu, F., 2019. Right-lateral strike-slip faulting and related basin formations in the Turkish–Iranian plateau. *Developments in Structural Geology and Tectonics*, 3, 101-130: Elsevier.

Jackson, J., 1992. Partitioning of strike-slip and convergent motion between Eurasia and Arabia in eastern Turkey and the Caucasus. *Journal of Geophysical Research: Solid Earth*, 97, 12471-12479

Jackson, J., McKenzie, D., 1984. Active tectonics of the Alpine—Himalayan Belt between western Turkey and Pakistan. *Geophysical Journal International*, 77, 185-264.

Jackson, J., Priestley, K., Allen, M., Berberian, M., 2002. Active tectonics of the south Caspian basin. *Geophysical Journal International*, 148, 214-245.

Karimzadeh, S., Cakir, Z., Osmanoğlu, B., Schmalzle, G., Miyajima, M., Amiraslanzadeh, R., Djamour, Y., 2013. Interseismic strain accumulation across the North Tabriz Fault (NW Iran) deduced from InSAR time series. *Journal of Geodynamics*, 66, 53-58.

Khorrami, F., Vernant, P., Masson, F., Nilfouroushan, F., Mousavi, Z., Nankali, H., Saadat, S. D., Walpersdorf, A., Hosseini, S., Tavakoli, P., Aghamohammadi, A., Alijanzade, M., 2019. An up-to-date crustal deformation map of Iran using integrated campaign-mode and permanent GPS velocities. *Geophysical Journal International*, 217, 832-843.

Malekshahian, Z., Naeeni, M. R., 2018. Deformation analysis of Iran Plateau using intrinsic geometry approach and C1 finite element interpolation of GPS observations. *Journal of Geodynamics*, 119, 47-61.

Masson, F., Anvari, M., Djamour, Y., Walpersdorf, A., Tavakoli, F., Daignières, M., Nankali, H., Van Gorp, S., 2007. Large-scale velocity field and strain tensor in Iran inferred from GPS measurements: new insight for the present-day deformation pattern within NE Iran. *Geophysical Journal International*, 170, 436-440.

Masson, F., Djamour, Y., Van Gorp, S., Chéry, J., Tatar, M., Tavakoli, F., Nankali, H., Vernant, P., 2006. Extension in NW Iran driven by the motion of the South Caspian Basin. *Earth and Planetary Science Letters*, 252, 180-188.

Masson, F., Lehujeur, M., Ziegler, Y., Doubre, C., 2014. Strain rate tensor in Iran from a new GPS velocity field. *Geophysical Journal International*, 197, 10-21.

Nilforoushan, F., Masson, F., Vernant, P., Vigny, C., Martinod, J., Abbassi, M., Nankali, H., Hatzfeld, D., Bayer, R., Tavakoli, F., Ashtiani, A., Doerflinger, E., Daignières, M., Collard, P., Chéry, J., 2003. GPS network monitors the Arabia-Eurasia collision deformation in Iran. *Journal of Geodesy*, 77, 411-422.

Rastbood, A., Voosoghi, B., 2011. Extension and slip rate partitioning in NW Iran constrained by GPS measurements. *Journal of Geodetic Science*, 1, 286-304.

Su, Z., Wang, E.-C., Hu, J.-C., Talebian, M., Karimzadeh, S., 2016. Quantifying the Termination Mechanism Along the North Tabriz-North Mishu Fault Zone of Northwestern Iran via Small Baseline PS-InSAR and GPS Decomposition. *IEEE Journal of Selected Topics in Applied Earth Observations and Remote Sensing*, 10, 130-144.

Vernant, P., Nilforoushan, F., Hatzfeld, D., Abbassi, M., Vigny, C., Masson, F., Nankali, H., Martinod, J., Ashtiani, A., Bayer, R., Tavakoli, F., Chéry, J., 2004. Present-day crustal deformation and plate kinematics in the Middle East constrained by GPS measurements in Iran and northern Oman. *Geophysical Journal International*, 157, 381-398.

Walpersdorf, A., Manighetti, I., Mousavi, Z., Tavakoli, F., Vergnolle, M., Jadidi, A., Hatzfeld, D., Aghamohammadi, A., Bigot, A., Djamour, Y., Nankali, H., Sedighi, M., 2014. Present-day kinematics and fault slip rates in eastern Iran, derived from 11 years of GPS data. *Journal of Geophysical Research: Solid Earth*, 119, 1359-1383.

Zarifi, Z., Nilfouroushan, F., Raeesi, M., 2014. Crustal stress map of Iran: insight from seismic and geodetic computations. *Pure and Applied Geophysics*, 171, 1219-1236.